EFFECT OF SCANNING SPEED TREATMENT ON THE MICROSTRUCTURE, MICROHARDNESS, WEAR AND CORROSION BEHAVIOUR OF LASER METAL DEPOSITED Ti–6Al–4V/TiC COMPOSITE

R. M. MAHAMOOD [1,2], *E. T. AKINLABI* [1]

[1] *Department of Mechanical Engineering Science, University of Johannesburg, South Africa;*
[2] *Department of Mechanical Engineering, University of Ilorin, Nigeria*

The influence of scanning speed on the microstructure, microhardness, wear and corrosion resistance behaviour of titanium alloy composite (Ti–6Al–4V/TiC composite) produced using laser metal deposition process was investigated. Rofin Sinar Nd-YAG laser was used to produce the samples at a laser power of 2.5 kW, powder flow rate of 2 g/min, and gas flow rate of 2 l/min. The scanning speed was varied between 0.005 and 0.050 m/s. The microstructural studies were carried out using optical microscope and scanning electron microscope. The microhardness profiling was done using Vickers microhardness tester at a load of 500 g and a dwell time of 15 s. The dry sliding wear of the composite was investigated using a ball-on-disk tribometer at a load range of 25 N. The corrosion behaviour was evaluated in 3.5% NaCl solution using potentiodynamic polarization measurement method. Unmelted carbide particles, as well as dendritic TiC were used. The percentage composition and distribution of all these particles were found to change as the scanning speed was varied. The microhardness was found to increase with increasing scanning speed. The wear volume produced was found to decrease as the scanning speed increased. The electrochemical behaviour of the composites showed that, as the scanning speed was increased, the corrosion potential and corrosion rate was found to be reduced.

Keywords: *additive manufacturing, corrosion, microstructure, microhardness, titanium alloy composite, wear.*

Titanium and titanium alloys have been favored in many applications because of the attractive properties they possess. Such properties include high strength to weight ratio, high modulus of elasticity, biocompatibility and high temperature performance [1]. Titanium and its alloys find their applications in industries such as aerospace, biomedical, chemical, energy, electronics, and defense due to their excellent properties [2]. Ti–6Al–4V is the most commonly used titanium alloy especially for aeronautical applications due to its super-plasticity, low weight, and high mechanical strength [3]. It is often referred to as the workhorse in the industry. However, in some applications where some service requirements needs to be met, such as the material coming in contact with other materials or in some working environment, the wear resistance property of Ti–6Al–4V is found to be poor as were as the corrosion resistance which makes them to lose their strength and fail [4]. Hence there is need for surface modification in order to improve the wear and corrosion resistance. A number of surface modifications of titanium have appeared in the literature [5]. Surface modification in the form of metal matrix composite is gaining more popularity in the research community because of the improved properties that are different from any of the constituent materials such as, very high hardness, improved wear resistance and corrosion resistance [6]. Different surface modification techniques have been used in the literature, namely: chemical vapour deposition, physical vapour deposition, thermal spray, plasma spray and laser metal deposition [5, 7, 8]. Among all these techniques, laser metal deposition provides an additional capability

Corresponding author: R. M. MAHAMOOD, e-mail: mahamoodmr2009@gmail.com

of achieving surface modification as well as building the component in one single operation. Also, owing to the fact that titanium and its alloys are considered as difficult to manufacture material because of their peculiar chemical property of the material having great affinity for other materials [9], laser metal deposition process is an excellent alternative manufacturing process for the material.

Laser additive manufacturing belongs to the directed energy deposition class of additive manufacturing technology which can fabricate parts no matter of the complexity directly from the three dimensional computer aided design model of the part by addition of materials in a layer wise fashion [10]. Laser metal deposition process is also useful in the repairs of engineering components which were in the past prohibitive or difficult to repair [11] and in the production of functionally graded materials [12, 13]. Although a lot of investigations on the wear and corrosion behaviour of laser metal deposited titanium and titanium alloy composite have been reported in the literature [14–19], the study of corrosion behaviour of laser metal deposited Ti–6Al–4V/TiC composite on Ti–6Al–4V substrate is scarce. Also the process parameters have a great influence on the evolving properties in laser metal deposition process as well as in the economy of the process [20, 21].

In this study, the microstructure, the micro hardness, the wear and corrosion behaviour of Ti–6Al–4V/TiC composite produced by laser metal deposition process is thoroughly investigated. Nd-YAG laser was used for the deposition process; wear testing was carried out in dry environment and the electrochemical technique was used for corrosion behaviour study in 3.5% NaCl solution. The influence of the scanning speed on all the aforementioned properties was investigated and the results are presented and extensively discussed.

Materials and methods. ***Materials and laser metal deposition process.*** The powders used in this experiment are the Ti–6Al–4V and TiC. The Ti–6Al–4V is of 99.6% purity and with a particle size range between 150 and 200 μm. The TiC powder is of 99.5% purity and powder particle size of below 60 μm. Hot rolled Ti6Al4V plate was used as a substrate and is of 99.6% purity. 4.0 KW Rofin Sinar Nd-YAG laser was used for the laser metal deposition process. The laser was controlled with a Kuka robot carrying the laser head and attached with coaxial powder in its end effector. A two hopper powder delivery system was connected to the laser head through the co axial powder nozzles. The two powders (Ti–6Al–4V and TiC powder) were put in each of the two hoppers separately and the powder flow rate of the two hoppers were maintained at 2 g/min giving rise to a composite of 50 vol.% TiC and 50 vol.% Ti–6Al–4V for the composite. The substrate was sand blasted to roughen the surface of the substrate and cleaned with acetone to degrease it before the deposition process began. The laser focal distance was kept at 195 mm at a spot ∅2 mm. The laser power, the powder flow rate, and the

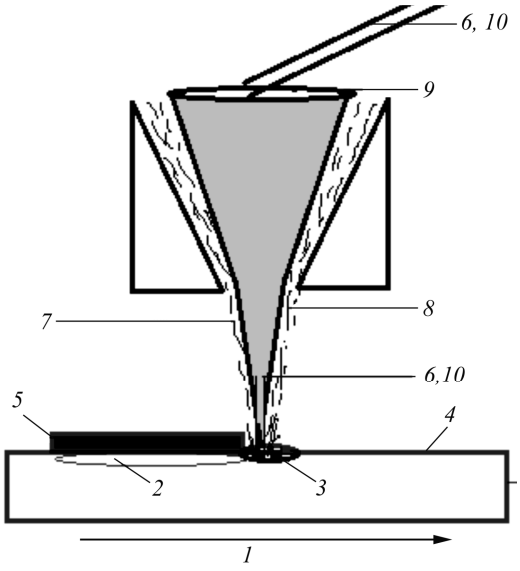

Fig. 1. Schematic diagram of laser metal deposition process [15]: *1* – processing direction; *2* – heat affected zone; *3* – melt pool; *4* – substrate; *5* – deposit; *6, 10* – laser beams; *7, 8* – Ti–6Al–4V and TiC powders; *9* – lens.

gas flow rate were kept at constant values of at 2.5 kW, 2.88 g/min and 2 l/min respectively. The scanning velocity was varied 0.005…0.050 m/s, step 0.005. The improvised glove box was filled with Argon gas to keep the oxygen level below 10 PPM. The Argon gas was also used to shield the powders in the hopper and the nozzles. This is to prevent the powder and the deposited samples from the environment attack.

The laser metal deposition process was achieved by creating a melt pool on the substrate by the laser beam and the powders were delivered into the melt pool through the coaxial nozzles. As the melt pool solidifies a track of the composite is seen on the laser path. The schematic diagram of the laser metal deposition process is shown in Fig. 1. Multiple tracks of the composite were deposited at each processing parameters and at a 50% overlap percentage.

Microstructural characterization and microhardness profiling. The samples for the microstructure examination were sectioned perpendicular to the deposition direction and mounted in resin. The samples were ground and polished according to the standard metallurgical preparation of titanium and its alloys. The polished samples were etched using the Kroll's reagent. The microstructures were observed using optical microscopy by Olympus BX51M. High magnification microstructural observation was done using Scanning Electron Microscopy (SEM) by Tescan, equipped with Oxford Energy Dispersion Spectrometry. The phases present are studied using the X-ray diffractometer by Ultima IV.

The microhardness indentations were measured using the MH-3 Vickers microhardness tester by Metkon. A load of 500 g was used for the microhardness test with a dwell time of 15 s. The space between the indentations was maintained at 10 μm (equivalent to more than twice the diameter of indentation).

Dry sliding wear test electrochemical corrosion test. The dry wear test was conducted using a ball on disk arrangement on a tribometer by Cert. Tungsten carbide of 10 mm diameter was used as the counter body at a load of 20 N with reciprocating frequency of 20 Hz, at a sliding distance of 2000 m. the wear volume was measured using the equation developed by [22].

The samples for electrochemical test were cut with a dimension of 1 cm by 1 cm. An insulated copper wire was attached to the back of the sample using aluminium tape to establish continuity between the sample and the copper wire. The samples were mounted with the deposited surface face down in the mounting cup in order to reveal the deposited part after mounting. The samples were allowed to solidify and then removed from the mounting cups. Only the deposited surface of area 1 cm^2 was exposed. The samples were ground and polished using 1200 grit SiC paper and 3 μm using diamond suspension. The samples were cleansed with ethanol before they are immersed in the 3.5% NaCl solution. The electrochemical tests were conducted in 3.5% NaCl solution (Ph of 6.24) at a room temperature of 23±1°C using a three-electrode system. The samples were the working electrode; the platinum rod was used as the counter electrode while the silver/silver chloride (Ag/AgCl) 3 M KCl was used as the reference electrode. The potentiodynamic polarization method was employed to study the general corrosion behaviour of the samples according to ASTM G 3-89 and ASTM 5-94 standards. The measurements were performed using the Auto lab potentiostat (PGSTAT30 computer controlled). The corrosion parameters were obtained by the analyses of the Tafel plot with the General Purpose Electrochemical Software version 4.9. The open circuit potential scan was performed for one hour for stabilization of the samples and followed by the linear polarization scan at a scan rate of 1 mV/S starting from −0.25 V with respect to the OCP measured value to +0.25 V with respect the OCP the measured value. The experiments were performed in triplicates to establish the reproducibility.

Results and discussion. The results are presented in three sub sections under the following headings: microstructural characterization of the laser deposited samples, microhardness and wear, and electrochemical analysis.

Microstructural characterization. The morphology of the Ti–6Al–4V powder is shown in Fig. 2*a*. The powders are spherically shaped which is typical of any gas atomized powders. Spherically shaped powders are laser friendly, as they aid in the absorption process of the laser beam which makes them to be more favored in laser metal deposition process. The morphology of the TiC powder is shown in Fig. 2*b*. The TiC powder was produced through milling process, being a hard powder, hence, the irregular shape structure. The microstructure of the Ti–6Al–4V substrate is shown in Fig. 2*c*. The microstructures revealed the alpha and beta phases. The alpha phases are light colored while the beta phase is dark colored. This microstructure is typical of any Ti6Al4V with these microstructures which are favored by the presence of both the alpha and beta stabilizers present in the alloy (i.e. the aluminium and vanadium).

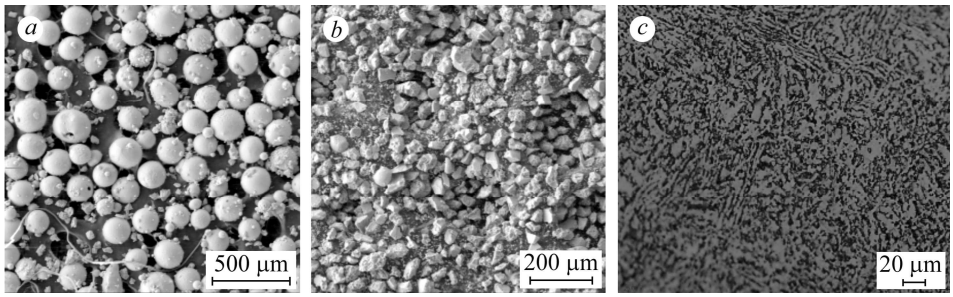

Fig. 2 SEM micrograph of: *a* – Ti–6Al–4V powder; *b* – TiC powder; *c* – Ti–6Al–4V substrate.

The micrograph of the laser deposited sample at the scanning speed of 0.01 m/s is shown in Fig. 3*a*. The micrograph was taken at low magnification to show the substrate, the transition zone and the deposited area.

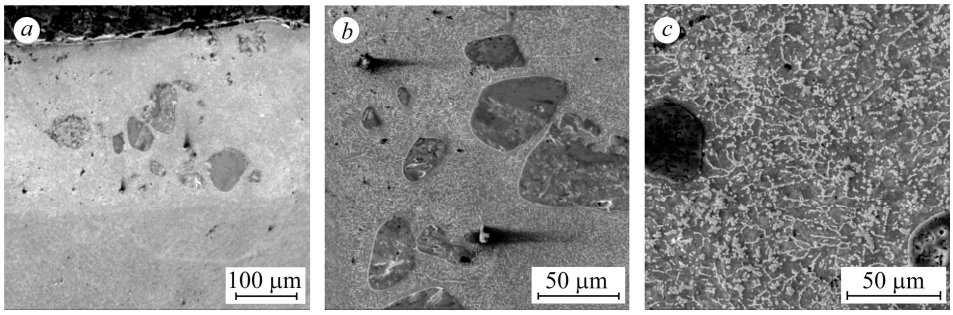

Fig. 3. SEM micrograph of sample at a scanning speed: *a* – 0.01 m/s; *b* – 0.015; *c* – 0.02 m/s.

This micrograph is similar for all the samples showing a very smooth transition from the substrate and the composite. It can be seen that there are some unmelted TiC (known as unmelted carbide (UMC)) particles in the microstructure. Though the TiC powders were not completely melted it is evident that the surface of the powder was melted giving the smoother curved shaped characteristic. This is clearly shown in Fig. 3*b* for the sample at the scanning speed of 0.015 m/s. The shapes of the unmelted carbide are still irregular but the edges are seen to be smoother as a result of surface melting occurring. The shape and sizes of these UMC were seen to be smoother and smaller at low scanning speed. This is because at low scanning speed the laser material interaction time is higher and there is a lot of surface melting of the TiC powder taking place. The other microstructures observed are the dendritic carbide and the re-solidified carbide as clearly shown for the sample produced at the scanning speed of 0.02 m/s (see Fig. 3*c*). The re-solidified carbides (RSC) are formed as a result of melting of the TiC powder which is precipitated during solidification. Some of these RSC grow to form the dendritic TiC which may happen when the solidification process and the

cooling process take a longer time to allow the grain growth. At low scanning speed the melt pool formed is larger and the solidification process also takes a longer time. The TiC precipitates now have enough time to undergo a dendritic growth. The formed dendritic TiC are coarser at lower scanning speed, this is because at low scanning speed the melt pool temperature is very high due to the large melt pool created by the prolonged interaction of the materials and the laser beam. The dendritic TiC is finer at higher scanning speed. These microstructures are definitely going to have effect on the microhardness, the wear resistance behaviour as well as the corrosion resistance behavior. The microhardness and wear are explained in the next subsection.

Microhardness and wear performance. The results of the average microhardness values and the wear volume loss are presented in Table 1. The microhardness was observed to be very high at the outer surface of all the samples. This is because of the rapid solidification occurring on the surface of the deposited track. The solidification in the core part takes longer time thus, lowering microhardness values in this region. The averages of these microhardness values are recorded. The Table shows that the microhardness reduces as the scanning speed increases. This phenomenon can be explained thus: at low scanning speed, the laser material interaction time is longer and the melt pool created by the laser beam on the substrate is also larger. The larger the melt pool, the longer the solidification process. As it was seen on the microstructure at low scanning speed, the quantity of the melted TiC is larger than at the low scanning speed. The melted TiC particles are precipitated as the RSC and the dendritic TiC. These particles in the microstructure give the required reinforcement to the composite, that is: the higher microhardness values at lower scanning speed. On the other hand, at higher scanning speed, the quantity of the UMC is larger, and the composite is relatively softer because of large quantity of the UMC in the matrix which is responsible for the lower microhardness values at a higher scanning speed. This behaviour is similar to the wear resistance behaviour.

Table 1. Microhardness and wear volume loss results

Sample	v_{scan}, m/s	Microhardness, HV	Wear volume loss, mm^3
A	0.005	500	0.135
B	0.01	489	0.129
C	0.015	480	0.1
D	0.02	472	0.098
E	0.025	460	0.092
F	0.03	441	0.091
G	0.035	433	0.087
H	0.04	427	0.082
I	0.045	416	0.076
J	0.05	398	0.065
Substrate	0	302	0.18

The wear volume loss is seen to reduce as the scanning speed increase. This is because, at low scanning speed, the large quantities of the RSC and the dendritic TiC as well as the coarseness of the dendrites cause the composite to be very hard (as shown in the microhardness result). This embrittles the composite because the RSC and the dendritic TiC are harder than the unmelted carbide particles. During sliding wear process, the harder RSC and UMC cut deeper into the surface, thereby aggravating the wear action. At higher scanning speed, the quantities of the UMC are larger and are easily ground into fine powder during the sliding wear action. These powders tend to

separate the sliding surface by forming a powder lubricant between the two surfaces. This action will tend to reduce the wear action, hence the lower wear volume loss is observed at higher scanning speed.

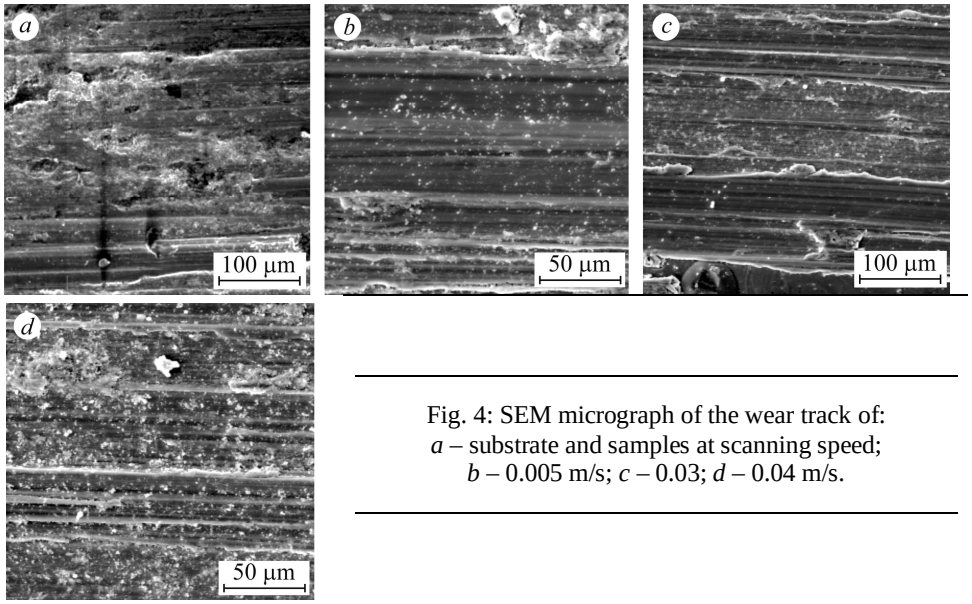

Fig. 4: SEM micrograph of the wear track of:
a – substrate and samples at scanning speed;
b – 0.005 m/s; *c* – 0.03; *d* – 0.04 m/s.

The worn tracks of the substrate, the samples at the scanning speed of 0.005, 0.03 and 0.045 m/s are shown in Fig. 4. The wear action that is seen on the substrate (see Fig. 4*a*) are ploughing groves produced as a result of the cutting of the work hardened debris that due to sliding action progresses. The debris become very hard as they are work hardened thereby forming a three body motion and cutting and tearing the surfaces. The wear of the sample at a scanning speed of 0.005 m/s is shown in Fig. 4*b*, wear behaviour is similar to that of the substrate only that the materials cutting the surface are the RSC and the dendritic TiC. The wear scar shown in Fig. 4*c* is for the sample at a scanning speed of 0.03 m/s. The wear scare is seen to be improved when compared to the scars shown in Figs. 4*a* and *b*. This is because there is a moderate amount of UMC as well as the RSC and dendritic TiC. The RSC and the dendritic carbides are cutting groves in the surface and at the same time the UMC in the matrix are being ground into powder as the sliding action progresses which later tend to inhibit the wear action. The wear scar of the sample at a scanning speed of 0.4 m/s is shown in Fig. 4*d*. It is seen to contain finely ground UMC particles that tend to form a protective layer between the two surfaces sliding against each other. The ploughing groves are seen in the microstructure caused by the RSC and the dendritic TiC. Because they are in a small quantity, there effects are not great when compared to those of the samples at low scanning speeds. Also the powder lubricant formed by the larger quantity of the UMC particles prevents the further action of the RSC and dentritic TiC on the sliding surfaces.

***Electrochemical analysis*.** The samples for the electrochemical analysis were cut as a square of 1×1 cm and mounted in cold epoxy resin, mechanically polished using various grades of SiC paper down to 1200 grit and then polished using 1 μm diamond were paste. The samples were washed with ethanol before they inserted into the cell. The open circuit potential (OCP) measurements at the scanning speed of 0.03 m/s was carried out in 3.5% NaCl solution for one hour. The potential initially increased and then stabilized after 1 h.

The OCP remains stable within an hour of the immersion time for all the samples. This shows that there is a continuous passivation that occurs as a result of the formation of the oxide protective layer on the samples surface. The average values of corro-

sion potential (E_{corr}) for all the samples are presented in Table 2. The graph of the E_{corr} against scanning speed is shown in Fig. 5*a*. The E_{corr} is seen to move towards the noble values as the scanning speed increases with the sample at the scanning speed of 0.05 m/s having the highest OCP value of –0.02 V and that of the scanning speed of 0.005 m/s has the lowest OCP value of –0.0772 V. The reason for this could be attributed to the presence of a larger percentage of the RSC and the dendritic TiC at low scanning speed Thereby aggravating corrosion effect is noticed. All the samples exhibit nobler values when compared to the OCP of the substrate of –0.1248 V.

Table 2. Electrochemical data obtained from the analysis of the OCP against time and linear polarization curves recorded at 1 mV·s^{-1}

Sample	v_{scan}, m/s	E_{corr}, V	i_{corr}, μA/cm^2	v_{corr}, mm/year
A	0.005	–0.0772	0.0277	0.3239
B	0.01	–0.0732	0.0233	0.27138
C	0.015	–0.07	0.0181	0.2109
D	0.02	–0.0655	0.0155	0.1802
E	0.025	–0.0612	0.0112	0.1313
F	0.03	–0.0513	0.0088	0.1039
G	0.035	–0.045	0.0043	0.05087
H	0.04	–0.0359	0.0014	0.01541
I	0.045	–0.0268	0.0011	0.01173
J	0.05	–0.02	0.0008	0.008477
Substrate	0	–0.1248	0.0335	0.3911

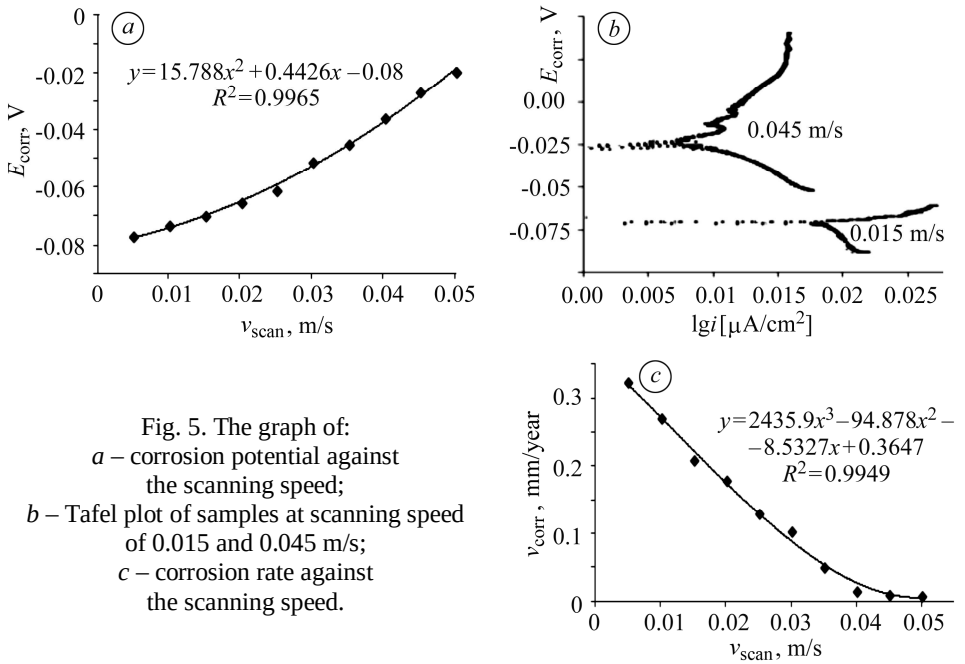

Fig. 5. The graph of:
a – corrosion potential against the scanning speed;
b – Tafel plot of samples at scanning speed of 0.015 and 0.045 m/s;
c – corrosion rate against the scanning speed.

The potentiodynamic polarization measurements were conducted to determine the active-passive characteristics of samples at different scanning speeds. Potentiodynamic polarization tests were performed using the scan rate of 1 mV/s, with ±250 mV from their OCP values in the cathodic and anodic directions. The corrosion potential, the

corrosion current density and the corrosion rates were calculate from the Tafel plots obtained for all the samples and the results are presented in Table 2. The Tafel plot of samples at scanning speeds of 0.015 and 0.045 m/s is shown in Fig. 5*b*. The graph of corrosion rate against the scanning speed is shown in Fig. 5*c*. The corrosion rate is found to decrease with increase in the scanning speed. This can be attributed to the fact that the moderate quantity of the UMC and RSC particles present in the samples at higher scanning speed may favor the increase in corrosion resistance due to the formation of the stronger protective oxides layer on the surface of the samples which tends to inhibit corrosion.

CONCLUSION

The microstructure, microhardness, wear and corrosion behavior of Ti–6Al–4V/TiC composite have been thoroughly studied. The electrochemical analysis was conducted in 3.5% NaCl solutions using potentiodynamic techniques. The higher the scanning speed, the higher the quantity of UMC and lower the RSC and dendritic TiC. These are seen to have improved the microhardness, the wear resistance and the corrosion resistance behaviour of laser metal deposited Ti–6Al–4V/TiC composite. The microhardness decreases as the scanning speed increased, while the wear resistance was found to increase as the scanning speed grows. From the results of open-circuit potential measurements, of the laser metal deposited Ti–6Al–4V/TiC composite, the corrosion potential shifts steadily towards the nobler values as the scanning speed was increasing indicating the formation of a passive layer of the metal oxides. It was also observed that the corrosion density current, decreased with increasing the scanning speed and so the corrosion rate.

РЕЗЮМЕ. Досліджено вплив швидкості сканувальної обробки на мікроструктуру, мікротвердість, зношування та корозію композиту Ti–61–4V/TiC, отриманого лазерним осадженням. Для приготування зразків застосовано лазер компанії Rofin Sinar Md-YAG потужністю 2,5 kW зі швидкістю заповнення порошком 2 g/min та швидкістю газового потоку 2 l/min. Швидкість напилювання змінювалася від 0,005 до 0,050 m/s. Для мікроструктурних досліджень використано оптичну та сканівну електронну мікроскопію. Мікротвердість виміряно давачем Вікерса за навантаження 500 g та часу витримки 5 s. Зношування композиту за сухого тертя досліджено методом потенціодинамічного поляризаційного вимірювання за принципом “кулька по диску” за навантаження 25 N. Корозійну поведінку вивчено у 3,5% NaCl потенціодинамічним поляризаційним методом. Використано нерозплавлені частинки карбіду, а також дендритні частинки TiC. Процентний склад та розподіл цих частинок змінювався зі швидкістю напилення, зокрема мікротвердість зростала, а об’єм зношування зменшувався. Крім того, з її підвищенням корозійний потенціал та швидкість корозії композитів зменшуються.

РЕЗЮМЕ. Исследовано влияние скорости сканирующей обработки на микроструктуру, микротвердость, износ и коррозию композита Ti–61–4V/TiC, полученного лазерным осаждением. Для приготовления образцов применен лазер компании Rofin Sinar Md-YAG мощностью 2,5 kW со скоростью заполнения порошком 2 g/min и скоростью газового потока 2 l/min. Скорость напыления изменялась от 0,005 до 0,050 m/s. Для микроструктурных исследований использована оптическая и сканирующая электронная микроскопия. Микротвердость измерена датчиком Викерса при нагрузке 500 g и времени выдержки 5 s. Износ композита при сухом трении исследован методом потенциодинамического поляризационного измерения по принципу “шарик по диску” при нагружении 25 N. Коррозионное поведение изучено в 3,5% NaCl потенциодинамическим поляризационным методом. Использованы нерасплавленные частицы карбида, а также дендритные частицы TiC. Процентный состав и распределение этих частиц изменялся со скоростью напыления, в частности, микротвердость увеличивалась, а объем износа уменьшался. Кроме того, с ее увеличением коррозионный потенциал и скорость коррозии композитов уменьшались.

Acknowledgments. This work is supported by the Council of Scientific and Industrial Research (CSIR) National Laser Centre, Rental Pool Programme, Pretoria, South Africa; University of Johannesburg Research Council and L’Oreal-UNESCO for Women in Science.

1. *Wear* characteristics of Ti–6Al–4V alloy at 20–400°C / X. H. Cui, Y. S. Mao, M. X. Wei, and S. Q. Wang // Tribology Trans. – 2012. – **55**, № 2. – P. 185–190.
2. *Imam M. A. and Froes F. H. S.* Low cost titanium and developing applications // JOM. – 2010. – **62**, № 5. – P. 17–20.
3. *Titanium* alloys for aerospace applications / M. Peters, J. Kumpfert, C. H. Ward, and C. Leyens // Adv. Eng. Mat. – 2003. – **5**, № 6. – P. 419–427.
4. *Lubricated* rolling sliding behaviour of ion nitride and untreated Ti.6Al.4V / G. Straffelini, A. Andriani, B. Tesi, A. Molinari, and E. Galvanetto // Wear. – 2004. – **256**, № 3–4. – P. 346–352.
5. *Research* progress on laser surface modification of titanium alloys / Y. S. Tian, C. Z. Chen, S. T. Li, and Q. H. Huo // Appl. Surf. Sci. – 2005. – **242**. – P. 177–184.
6. *Wear* and friction coefficient of particle reinforced Ti-alloys / C. Poletti, A. Merstallinger, T. Schubert, W. Marketz, and H. P. Degischer // Mat. Sci. and Eng. Techn. – 2004. – **35**. – P. 741–749.
7. *Surface* modification of the titanium implant using TEA CO2 laser pulses in controllable gas atmospheres – Comparative study / J. Ciganovic, J. Stasic, B. Gakovic, M. Momcilovic, D. Milovanovic, M. Bokorov, and M. Trtica // Appl. Surf. Sci. – 2012. – **258**, № 7. – P. 2741–2748.
8. *Weng F., Chen C., and Yu H.* Research status of laser cladding on titanium and its alloys: a review // Materials and Design. – **58**. – P. 412–425.
9. *Machado A. R. and Wallbank J.* Machining of titanium and its alloys: a review // Proc. Institution of Mechanical Engineers. P. B: Management and Eng. Manufact. – 2005. – **204**. № 11. – P. 53–60.
10. *Additive* manufacturing: status and opportunities / J. Scott, N. Gupta, C. Wember, S., Newsom T. Wohlers, and T. Caffrey // Science and Technology Policy Institute, – 2012. Available from: https://www.ida.org/stpi/occasionalpapers/papers/AM3D_33012_Final.pdf (Accessed on 11 July 2016).
11. *Graf B., Gumenyuk A., and Rethmeier M.* Laser metal deposition as repair technology for stainless steel and titanium alloys // Phys. Proc. – 2012. – **39**. – P. 376–381.
12. *Functionally* graded material: an overview / R. M. Mahamood, E. T. Akinlabi, M. Shukla, and S. Pityana // Lecture Note in Eng. – 2012. – **3**. – P. 1593–1597.
13. *Mahamood R. M. and Akinlabi E. T.* Laser metal deposition of functionally graded Ti6Al4V/TiC // Materials and Design. – 2015– **84**. – P. 402–410.
14. *Scanning* Velocity Influence on Microstructure, Microhardness and Wear Resistance Performance on Laser Deposited Ti6Al4V/TiC Composite / R. M. Mahamood, E. T., Akinlabi M., Shukla and S. Pityana // Materials and Design. – 2013. – **50**. – P. 656–666.
15. *Characterization* of Laser Deposited Ti6A4V/TiC Composite / R. M. Mahamood, E. T., Akinlabi M. Shukla, and S. Pityana // Lasers in Eng. – 2014. – **29**, № 3–4. – P. 197–213.
16. *Effect* of ZrO_2 addition on the dry sliding wear behaviour of laser clad Ti–6Al–4V alloy / B. A. Obadele, A. P. Andrews, P. A. Olubambi, M. T. Mathew, and S. Pityana // Wear. – 2015. – **328–329**. – P. 295–300.
17. *Electrochemical* behaviour of laser-clad Ti–6Al–4V with CP Ti in 0.1 M oxalic acid solution / B. A. Obadele, P. A. Olubambi, A. P. Andrews, S. Pityana, and M. T. Mathew // J. Alloys and Comp. – 2015. – **646**. – P. 753–759.
18. *Effects* of Ti and TiC ceramic powder on laser-cladded Ti–6Al–4V in-situ intermetallic composites / O. F. Ochonogor, C. Meacock, M. Abdulwahab, S. L. Pityana, and A. P. I. Popoola // J. Appl. Surf. Sci. – 2012. – **263**, № 15. – P. 591–596.
19. *Erosion* resistance of laser clad Ti–6Al–4V/WC composite for water jet tooling / P. K. Farayibi, J. W. Murray, L. Huang, F. Boud, P. K. Kinnell, and A. T. Clare // J. Mat. Proc. Techn. – 2014. – **214**, № 3. – P. 710–721.
20. *Effect* of laser power on material efficiency, layer height and width of laser metal deposited Ti–6Al–4V / R. M. Mahamood, E. T. Akinlabi, M. Shukla, and S. Pityana // Lecture Note in Eng. and Comp. Sci. – 2012. – P. 1433–1438.
21. *Material* efficiency of laser metal deposited Ti–6Al–4V: Effect of laser power / R. M. Mahamood, E. T. Akinlabi, M. Shukla, and S. Pityana // Eng. Letters. – 2013 – **21**, № 1. – Available online at http://www.engineeringletters.com/issues_v21/issue_1/EL_21_1_03.pdf
22. *Sharma S., Sangal S., and Mondal K.* On the optical microscopic method for the determination of ball-on-flat surface linearly reciprocating sliding wear volume // Wear. – 2013. – **300**, № 1–2. – P. 82–89.

Received 10.11.2015